LNF–97/042

Sinbad: The New Powerful Infrared Source from the DAΦNE Storage Ring

A. Marcelli, E. Burattini, C. Mencuccini, A. Nucara, P. Calvani, S. Lupi, M. Sanchez del Rio

Proc. Accel. Based Infrared Sources and Appl., 3153, 21–32
(San Diego, CA. 29–30 July 1997)

PROCEEDINGS OF SPIE REPRINT

SPIE—The International Society for Optical Engineering

Reprinted from

Accelerator-Based Infrared Sources and Applications

29–30 July 1997
San Diego, California

Volume 3153

SINBAD: THE NEW POWERFUL INFRARED SOURCE FROM THE DAΦNE STORAGE RING

A. Marcelli[a], E. Burattini[a,b], C. Mencuccini [a,c], A. Nucara[d], P. Calvani[d], S. Lupi[d] and M. Sanchez del Rio[e]

[a]INFN, Laboratori Nazionali di Frascati, C.P.13, 00044 Frascati, Italy
[b]Facolta' di Scienze, Universita' di Verona, 37100 Verona, Italy
[c]Dipartimento di Energetica, Universita' di Roma "La Sapienza", 00185 Roma, Italy
[d]INFM - Dipartimento di Fisica, Universita' di Roma "La Sapienza", 00185 Roma, Italy
[e]European Synchrotron Radiation Facility, BP 220, 38043 Grenoble-Cedex, France

ABSTRACT

We report on the status of the first Italian Infrared Synchrotron Radiation Beamline SINBAD (Synchrotron INfrared Beamline At DAΦNE), that has been designed to work at wavelengths greater than 10 μm. SINBAD is being installed on DAΦNE, the new collider of the Laboratori Nazionali di Frascati designed to work at 0.51 GeV with a beam current of 2 to 5 A. The infrared radiation extracted from a bending magnet under an angle of 50x50 mrad will be two orders of magnitude more brilliant than that of a black body at 2000 K at a wavelength of 100 μm. The beamline layout, which consists of two plane mirrors, two toroidal mirrors and one aspherical mirror, has been designed by ray tracing simulation. In this layout one ellipsoid focuses the radiation on a wedged CVD diamond-film window, the beam is then re-focused again on the entrance of an interferometer. With a calculated transmittance of the optics between 60% and 80% at 50 μm, this beamline will allow experiments which require a very high brilliance in the far infrared.

Keywords: Synchrotron Radiation, Infrared beamline, Mirror optics, Diamond windows.

1. INTRODUCTION

Synchrotron radiation (SR) is emitted by relativistic charges whenever they travel along a curved path. Due to relativistic effects, SR is emitted in a cone centered along the instantaneous velocity vector of the particles with a divergence which grows with the radiation wavelength. However, because of its high intensity and small divergence SR is a high brilliant source in the ultraviolet, soft x-ray and x-ray range where it is applied to the investigation of the structural and electronic properties of matter. The applications range from materials science to earth science, chemistry, biology, medical research and industrial processes.

Altough the use of SR in the infrared (IRSR) is relatively new (mid-eighties) it appears as one of the most promising applications of this source. Several IRSR facilities (at Brookhaven, Okasaki, Orsay, Daresbury and Lund) are already available at present, while others are being projected or are under construction.

DAΦNE (Double Annular Φ-factory for Nice Experiments) is the new electron-positron collider under construction in Frascati. This double ring is designed to produce Φ-mesons by annihilating electrons and positrons having an energy E of 0.51 GeV per beam. The critical energy of the DAΦNE spectral emission will consequently be very low. However, in no way this will reduce the infrared emission, as the intensity of this relativistic emission, for accelerated particles at energies E>0.51 GeV, in this range of wavelength and at fixed current, is independent of E. In addition, the IRSR is expected to be extremely intense for DAΦNE just because of the high current I of this collider (from 2 A at commissioning up to 5 A working in a topping up mode).

The present contribution will describe in some detail the optical layout and the expected performances of SINBAD, the IR beamline that we are going to install at DAΦNE. This beamline is designed to work in the wavelength range from 5 to 5000 μm, even if the transmission of shorter wavelengths will also be possible.

Other author information: (Send correspondence to A.M.)
R.S.: Email: marcelli@lnf.infn.it; Telephone: +39 6 94032357; Fax: +39 6 94032427

The scheme of the manuscript is the following. The parameters of DAΦNE which are relevant for the SR emission are reported in Section 2, and used therein to calculate the characteristics of the source in the IR domain. In Section 3 the characteristics and the ray tracing calculations of this beamline made by two separate sections will be described: the first one transmits the radiation from the bending magnet to a CVD wedged diamond window (DW), the second one transmits the radiation from the DW to the interferometer. Finally, preliminary results about the polarization properties of the radiation at the end of the beamline, and of the Actual Brilliance Ratio (ABR) in the sample position, obtained simulating the internal optics of the Michelson interferometer, will be also presented in Sections 4 and 5 respectively.

2. THE MACHINE PARAMETERS AND THE CHARACTERISTICS OF THE SOURCE

Table 1. DAΦNE single ring parameters.[1-4] ϵ_c and λ_c are the critical energy and critical wavelength respectively.

Energy	510 MeV	(γ=E/mc^2=10^3)	
Circumference	97.69 m		
Dipole bending radius	1.4 m	ϵ_c=208 eV	λ_c=59.6 Å
Dipole magnetic field	1.2 T		
Dipole bending angle	0.8 rad		
Wiggler bending radius	0.94 m	ϵ_c=311 eV	λ_c=39.9 Å
Wiggler magnetic field	1.8 T		
Wiggler length	2.0 m		
Wiggler period length	0.64 m	N_{period}=3	
Horizontal β-tune	4.87		
Vertical β-tune	4.85		
Momentum compaction	0.017		
Energy loss/turn (U_0)	9.3 keV		
Natural Horizontal Emittance	10^{-6} m rad		
Coupling coefficient k	0.01		
Natural Bunch length σ_z	0.81 cm		
Anomalous bunch length σ_z	3.0 cm		
Bunch separation	4.2 m		
Number of particles/bunch	9 10^{10}		
Number of bunches	$1 \div 120$		
Max. total average current	5.3 A		
RF freq.	368.25 MHz		
Harmonic number	120		
Max. SR Power/beam	49 kW		
Relative rms Energy spread	3.97 10^{-4}		
Anomalous Relative rms Energy spread	1.46 10^{-3}		
Damping Time	τ_s=17.8 msec	τ_x=36 msec	τ_y=35.7 msec
Total single beam lifetime	156 min		

For a SR source the number of photons emitted in a solid angle dθdψ and in a bandwidth $\delta\nu$=0.001ν is related to the beam current I and to the energy E by the equation[5]:

$$\frac{dF}{d\theta d\psi} = 1.327 \quad 10^{19} E^2 I \left(\frac{\lambda_c}{\lambda}\right)^2 K_{2/3}^2 \left(\frac{\lambda_c}{2\lambda}\right) \qquad photon/mrad^2/sec \tag{1}$$

where λ_c is the critical wavelength for the DAΦNE magnet and K is a modified Bessel function. The Actual Source Area (ASA) of the SR corresponds to the effective area of the source when all the possible broadening phenomena are taken into account. In the IR range it can be evaluated using the following relation[6]:

$$\Sigma_x \Sigma_y = 2\pi \sqrt{\sigma_x^2 + \sigma_r^2 + (\sigma_x^{geo})^2} \sqrt{\sigma_y^2 + \sigma_r^2 + (\sigma_y^{geo})^2} \qquad cm^2 \tag{2}$$

The terms σ_i, where the subscripts i=x,y refer to the horizontal and vertical size respectively, are the dimensions, as due to the electron beam size and divergence, while σ_r is the diffraction limited source size, that is a function of the intrinsic divergence of the radiation σ_ψ. The latter is strongly dependent by the wavelength, and in the infrared region ($\lambda \gg \lambda_c$) it may be written as[7]

$$\sigma_\psi(\lambda) = 0.816 \quad \left(\frac{\lambda}{\lambda_c}\right)^{0.354} \frac{10^{-3}}{E} \qquad rad \tag{3}$$

which shows a slightly differ behaviour respect to the x-ray region. As a consequence, the diffraction-limited size may be written as

$$\sigma_r(\lambda) = \left(\frac{\lambda}{4\pi\sigma_\psi}\right) \qquad rad \tag{4}$$

The terms σ_i^{geo} in Eq. 2 are due to the collection of a finite length of trajectory along the bending magnet and have been evaluated using mathematical expressions based on the approximation of an uniform distribution of the electron bunch along the trajectory.[6] From Equations 2, 3 and 4, one obtains for the source dimensions of the bending magnet of DAΦNE, the values reported in Table 2:

Table 2. Dimensions of the DAΦNE sources, including the diffraction term contribution.

λ (μm)	Σ_x (mm)	Σ_y (mm)
10	2.12	0.32
100	2.18	0.35
1000	2.28	0.76

The source was simulated by the ray tracing SHADOW program.[8] This code creates a collection of rays in a given region of the space (the source). Each ray is fully described by four vectors and two phases: the starting position $\vec{r}$, the wavevector $\vec{k}$, the electric vectors $\vec{A_s}$, and $\vec{A_p}$ and their associated phases ϕ_s and ϕ_p. The rays of the source are created using the Monte Carlo technique to sample the spatial, angular and spectral distributions of the synchrotron sources (a bending magnet in our case). The source is traced through an optical system consisting of a definite number of optical elements (i.e., mirrors, crystals, etc.). The mirror may have any mathematical surface (ellipsoidal, spherical, etc.). It is also possible to add to this ideal surface a mesh of imperfections. This feature allows us to add slope errors (measured or modeled), thermal deformations (calculated theoretically or by finite elements), gravity sag and/or any other figure error. In the IR region we found that SHADOW takes into account only the geometrical broadening and the beam size, while it does not consider the diffraction-limited contribution to the total size. This last is usually negligible at short wavelengths, certainly not in the IR domain. As a consequence, we selected as input for the ray tracing simulation of the source the data reported in Table 2, which include ad hoc, using Eq. 2, the diffraction limited contribution given by Eq. 4.

Table 3. Output parameters of the ray tracing code for the sources shown in Fig. 1. s'_x and s'_y are the width at half maximum of the non gaussian distributions.

λ (μm)	σ_x (cm)	σ_y (cm)	s'_x (rad)	s'_y (rad)
10	0.210	0.33	0.0058	0.010
100	0.216	0.46	0.0058	0.019
1000	0.226	0.81	0.0058	0.040

At DAΦNE the solid angle is limited by the geometrical constraint of the front-end flange (CF 63) placed at 1.2 m from the center of the virtual source, that limits the clear aperture to 50 mrad, both in the horizontal and in the vertical plane (see Table 3). For the simulations of SINBAD the horizontal collection angle has been set to 20

mrad, and the optical elements have been dimensioned to accept this divergence. It does not yield significant effects at short wavelengths (λ <200 μm), while it causes a significant intensity damping at higher wavelengths.[9] Then, selecting only 20 mrad could appear a limitation. However, this is the best choice to optimize our IRSR emission in the mid and far IR. Indeed, the large horizontal size of DAΦNE source increasing the horizontal collection angle, produces essentially a reduction of the brilliance.[6,9]

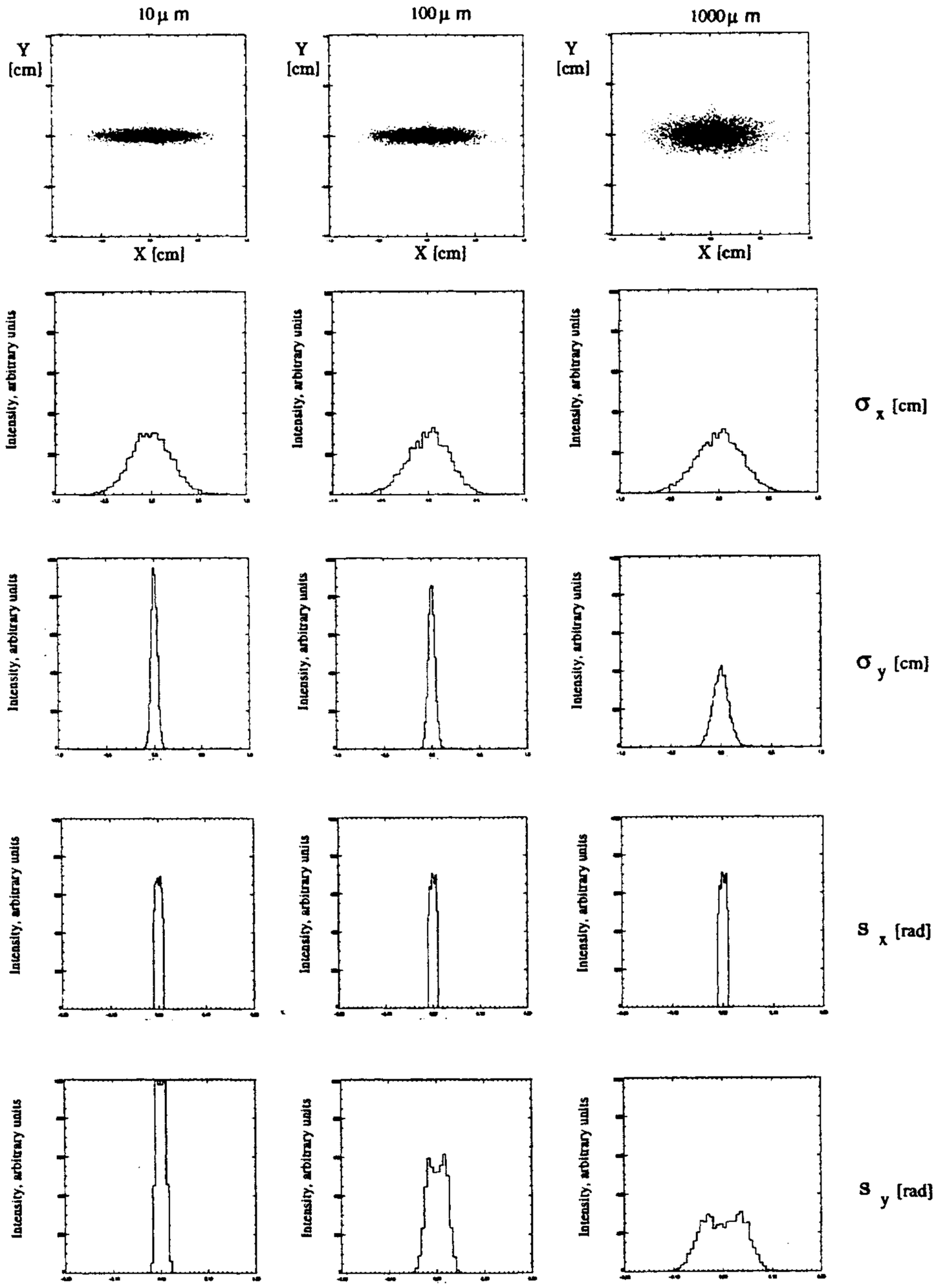

Fig 1. From left to right: plots of the source generated by SHADOW at 10 μm, 100 μm and 1000 μm. From top to bottom: distributions of the emitted intensity in the (x,y) plane, the spatial distributions in the vertical (y) and horizontal plane (x) and the angular distribution: s'_x (fixed to 20 mrad) and s'_y.

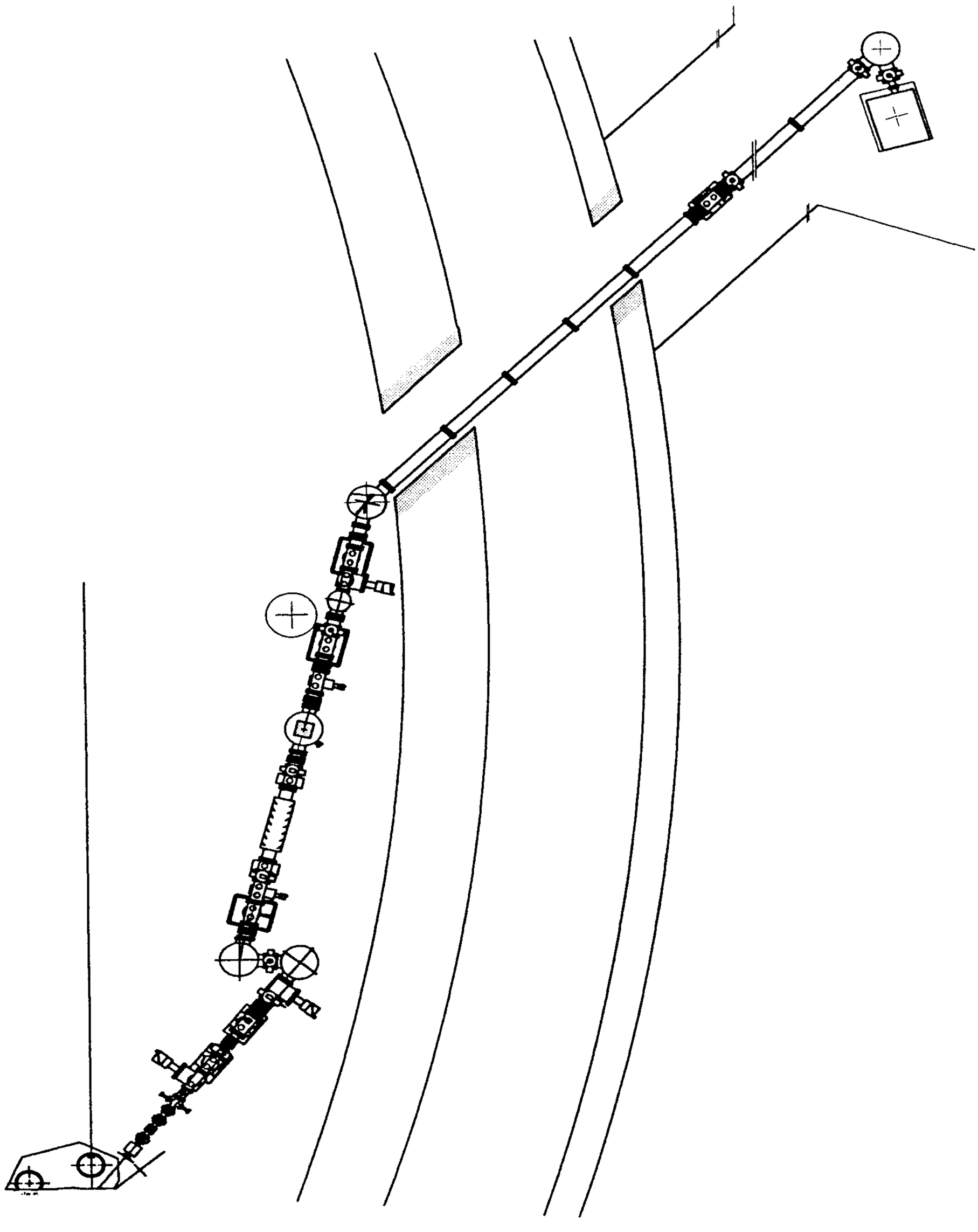

Fig 2. Layout of the SINBAD beamline.

3. THE SINBAD BEAMLINE

Starting from the first ray tracing of an optical layout for this beamline,[10] new designs of the layout due to additional constraints were considered. The main problem to solve on the design of a SR beamline in the IR domain is how to match the divergence of the IRSR to the f number of the entrance pupil of a Michelson interferometer. In addition, because the divergence grows with the wavelength, and in the far IR it becames very large (>100 mrad), it is not possible to transfer the radiation to the interferometer, that in our case will be located at about 20 m from the source, without focusing the radiation along its path. Moreover, because DAΦNE has been installed in the building, that hosted till May 1993 the ADONE ring, we also wanted to use the existing tunnel and its laboratory. This forced the layout to have a more complex scheme with additional deflections. The top wiev of the beamline is shown in Fig.2 where one can identify the location of the mirror chambers. The first straight part of the beamline is the front-end discussed in the next section. Then there is an extraction plane mirror and the ellipsoid that focuses the radiation with a demagnification 2:1 on the diamond window (DW), which separate this part of the beamline from a second section with a different vacuum regime. The deflection of this mirror in the horizontal plane, has been selected to allow the beamline to pass between the theodolite on the left and the shielding wall on the right. After the DW the beam is again divergent and a couple of mirrors (a toroid plus a plane) collimates the beam in both planes and lifts it up by 50 cm. A plane mirror, placed before the shielding wall, deflects the radiation through the shielding wall into the tunnel and to the experimental area where the last toroidal mirror focuses the radiation on the entrance pupil of the interferometer.

3.1. The UHV section

The first focusing section of the beamline, that contains the front-end and is kept under UHV is described here. The front-end is the essential set of elements that allow an easy operation of the beamline with no risk for the storage ring and for the users. The SINBAD front-end originates from the exit flange placed at 120 cm from the source, that defines the maximum clear aperture of the beam. Because all the elements of the first section of the beamline are directly connected to the ring, the vacuum regime required for this section is the ultra high vacuum (UHV). The length of the front-end is about 3 m, so that the first mirror has to be placed at 4.5 m from the source. It is the extraction mirror (M1). It is plane, made by Cu OFHC goald coated and contains three internal cooling channels, that should be used if necessary, to reduce the effects associated with the thermal load of the SR. Indeed, this mirror is the only one that has to withstand a not negligible amount of power. This mirror will deflect the beam by 55° in the horizontal plane towards an ellipsoidal mirror, placed 70 cm apart. The incidence angle of the elliptical mirror (M2) is 40°. The focal point of the ellipsoid is the small DW that separates and protects the UHV section of the beamline from the next section. Moreover, the focus produced at the DW location, represents for all the following optical elements, the effective source to be traced to the entrance pupil of the instrument. The second part of the beamline, described in the next section, is mantained at about 10^{-6} Torr to minimize the absorption loss of the IR radiation by residual gas contained in the long pipe to the interferometer. The ellipsoid used to focus the source has semi-major axes of 379 cm and semi-minor axes of 269 cm. Once fixed the mirror axes, the parameters defining the quality of the reflecting surface are the values of the slope error and of the roughness. In our case it is extremely important that the shape of the focus point produced by this optical element be the best and these two parameters, together with the accuracy in the profile manufacture, become essential. Typical values for the slope error and the roughness for x-ray optical elements are respectively $\leq$1 μrad and $\leq$5 $\AA$. In the IR range, the intrinsic dimension of the source hides the blur produced by the roughness. On the contrary to investigate the slope error contribution in our optical system, we generated virtual rough surfaces with variable slope errors Δ both in the sagittal and in the tangential planes. Tests made at several wavelengths, on the dimension of the beam in the focus point of the ellipsoid indicate that the divergence in the sagittal direction is unaffected by any reasonable value of the surface irregularity, while we observed an increase of the divergence at lower wavelenghts for slope error in the tangential plane of about 10 arcsec. As a consequence for the mirror tenders the slope error requirements, in the case of the non-plane mirrors, were fixed to <5 arcsec in the incidence plane and <50 arcsec in the sagittal one. In order to determine the influence of mechanical errors in the angular orientations of these mirrors we have also introduced in the ray tracing calculations small angular changes in the incidence angle. By selecting different errors in the incidence angles of the two mirrors M1 (plane) and M2 (ellipsoidal) we find that a deviation from the ideal condition should be observed only in the vertical direction (tangential plane) for angular errors greater than 0.2°. This can also help to evaluate the defocusing effect produced by small translations of the mirrors, i.e., the perturbation induced by small

displacements of the ellipsoidal mirror along its axes. In such case, the images produced by the ellipsoid on the DW location will appear at off-center positions, but the effects on the standard deviations of the horizontal and vertical ray distributions are negligible.

A further important effect we evaluated is the distortion of the mirrors induced by thermal load. Indeed, the power delivered to the optical elements may produce a distortion that increases the divergence of the reflected beam. For high energy storage rings, this phenomenon introduces severe limitations in the brilliance but, in our geometry and because the low energy of DAΦNE (E<0.7 GeV), the effect should be taken into account only for the first plane mirror. Our calculations performed for 0.75 GeV and I=1 A return a maximum power of about 150 W. At 0.51 GeV with a current >5 A the power is strongly reduced. At an incidence angle of 27.5° an energy cutoff of a few eV is obtained and, as a consequence, all the further optical elements receive a power load of the order of a few mW. The effect on the first mirror can be evaluated looking at the deformation of the spot size at the focus, as determined by the temperature gradient between the exposed top surface and the bottom side of the mirror, that should be cooled. One may then describe the mirror as a cylinder with a convex curvature along the vertical direction (tangential plane), while in the horizontal dimension it can be still considered as plane. Two materials are generally used to limit the distortion: SiC or Cu. They are both suitable whenever the thermal load is not negligible, for their low α/k value. Our M1 mirror is made of copper and its thermal conductivity k is 0.390 W/mm°C while the thermal expansion coefficient α is 16.79 10^{-6} mm/mm°C. At first order, if one considers an uniform illumination of the surface in the horizontal plane and neglects particular boundary conditions on the mirror, as well as possible distortions, the expression for the slope associated with the thermal bump is:[12]

$$\Delta = \left(\frac{\alpha}{k}\right)\frac{l}{2}Q \qquad mrad \tag{5}$$

where l is the mirror length and Q is the thermal load. For SINBAD the estimated power density is Q=8 Watt/cm^2 and for l=250 mm, we obtain for the Cu mirror Δ=0.43 mrad. This slope corresponds to an ideal deformation of radius R=581 m and broadens the spot on DW by 0.23 mm in the vertical direction at λ=50 μm. However, as the divergence of the IR radiation is intrinsically large, the effect of the thermal load on the brilliance become negligible for λ>50 μm.

3.2. The diamond window

One of the most important elements of our design is the diamond window. Here we briefly discuss its mounting and characteristics being our solution different from those used till now. Indeed, while the present operative IR beamlines use for the first window natural diamond crystals[13,14] or KRS-5 and silicon,[15] we have considered for SINBAD the possibility to use thin amorphous diamond films. We tested several chemical vapor deposition diamond (CVDD) plane windows, about 250 μm thick, and more recently also wedged windows supplied by DRUKKER, with a minimum tickness of 460 μm and 0.9° of wedge. Transmission experiments that are going to be presented in a forthcoming manuscript, showed for the latter that one can reduce to about <5% the interference of the multiple reflections typically observed at these wavelengths by using plane windows. The hardness of CVDD material (>7000 Knobs) is such that a pressure difference of 1 atm can be safely sustained over a diameter of 15 mm as that used for SINBAD, where a CVDD film is brazed on a double sided CF flange. Altough the hardness of a crystal is greater by a factor of two respect to a film, one significant advantage of CVDD window is its lower cost. A possible alternative to reduce interference fringes due to the multiple reflections is given by a flat window mounted at the Brewster angle.[13] However our tests show that the polarization and the divergence of the SR source are such that the efficiency of the wedged diamond windows is much higher under this respect.

3.3. The HV section

We describe here the final layout of the second section of the beamline which connects DW to the interferometer. Several constraints, i.e., the existing buildings, the aperture in the safety wall of the hall, the tunnel, the level of the ground, etc. limited the possible paths for SINBAD. Starting from the above boundary conditions, a general layout was sketched. Finally several solutions were figured out, with different performances and costs. These beamlines, characterized by the number of optical elements and by the number of aspherical optics, i.e., ellipsoids and paraboloids off-axis were evaluated using ray tracing. The top view of the geometrical path in Fig. 2 shows the complex optical layout selected. The starting consideration for the high vacuum section of this layout is that the

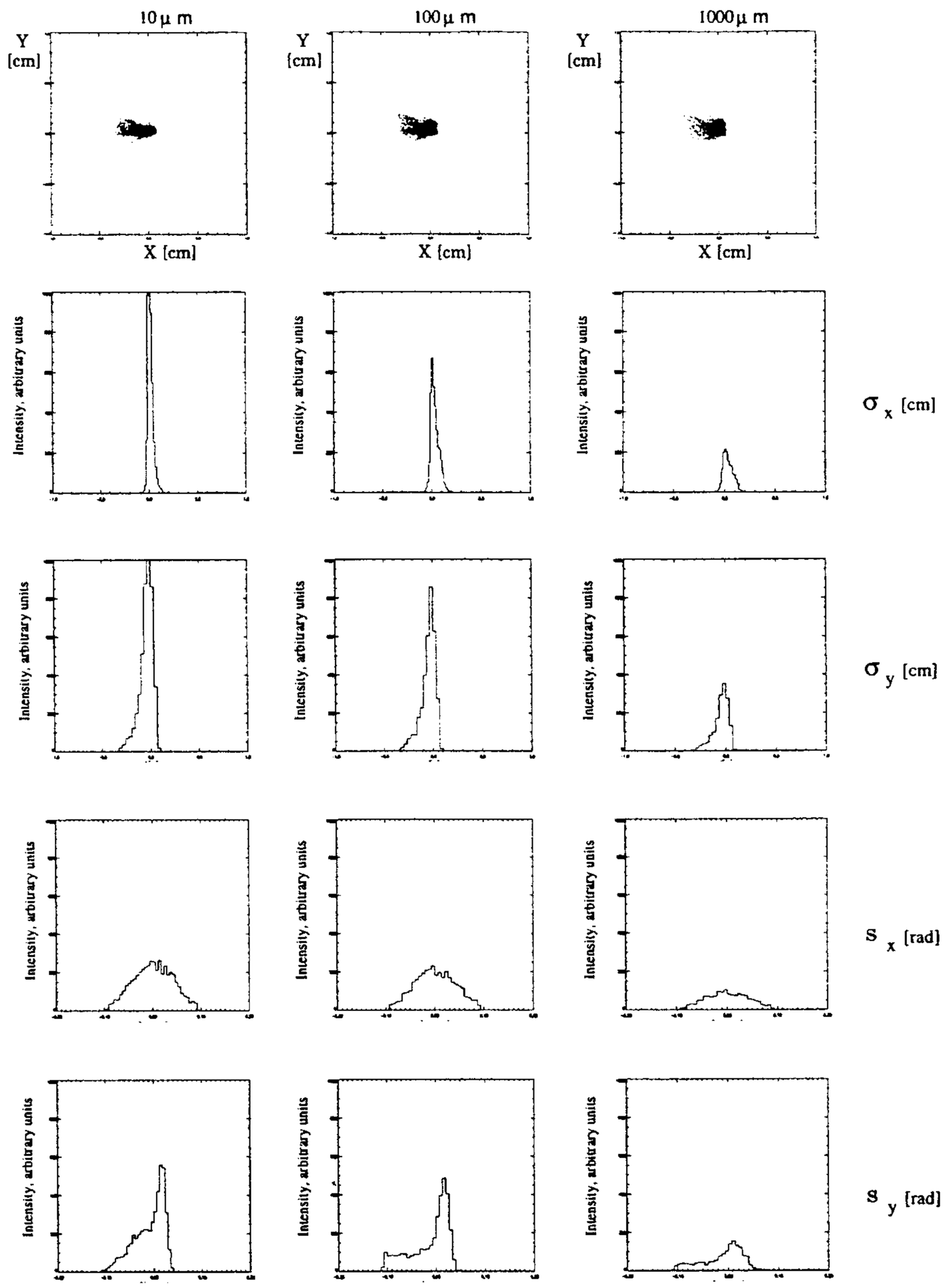

Fig 3. From left to right: plots of the image at the entrance pupil of the interferometer at 10 μm, 100 μm and 1000 μm. From top to bottom: distributions of the emitted intensity in the (x,y) plane, the spatial distributions in the vertical (y) and horizontal plane (x) and the angular distributions s'_x and s'_y.

source to be transferred to the sample is the image produced by the ellipsoidal mirror at the DW location. Taking into account the aberrations introduced by the different optical system the results of the ray tracing indicated as the best optical layout that which includes 4 parabolic off-axis mirrors.[16] In this layout the beam is transfered as a plane wave in both planes to reduce the effect of the large IRSR divergence and the possible influence of source instability. However, practical reasons suggested to replace this layout by a combination of simpler (in term of manufacture) elements, namely two planes and two spherical mirrors (see Table 4). The first mirror of the second section (M3) is

toroidal and is placed at 80 cm after DW. It vertically deflects the radiation by 90°. The second mirror (M4), plane, also deflects the radiation of 90° but in such a way that the reflected beam is parallel to the beam incident to M3 and to the horizontal plane. The third mirror (M5), also plane, deflects the beam in the horizontal plane into the tunnel and the experimental area, towards the final toroidal mirror (M6) at the end of this transfer line. This toroid deflects the radiation of 60° and focuses the radiation at 0.5 m from its pole. As a result, the beam is transfered as a plane wave in both directions and the final spot is well focused. However, because of the use of toroidal mirrors, geometrical aberrations may be clearly identified in the image. Plots of the image spots and divergences for this layout are given in Fig. 3, while ray tracing statistic is in Table 5.

Table 4. Parameters of the mirrors of the second section of SINBAD. The distance is measured from the previous optical element.

	Distance (cm)	Incidence angle	Figure	Major radius (cm)	Minor radius (cm)
M3	80	45°	TOROIDAL	226	113
M4	50	45°	PLANE		
M5	312	72.5°	PLANE		
M6	1300	30°	TOROIDAL	116	87

Table 5. Standard deviations for the images shown in Fig. 3. $s_y^{'}$ is the width at half maximum of the non-gaussian distributions. In the last column T is the estimated transmission.

λ (μm)	σ_x (cm)	σ_y (cm)	$\sigma_x^{'}$ (rad)	$s_y^{'}$ (rad)	T (%)
10	0.07	0.048	0.036	0.097	>99
100	0.07	0.072	0.037	0.136	83
1000	0.07	0.053	0.039	0.152	38

The focusing properties of this beamline appear quite satisfactory, and a small round spot is obtained. The first toroidal mirror (M3) does not produce strong aberrations, but the residual divergence of the beam after the reflection, generated a wave front not perfectly plane. The aberrations produced by the second toroid (M6) are stronger and responsible for the observed broadening of the image. Indeed, a comatic image is observed, even if the demagnification of the beamline is equal to 1 both in the sagittal and the tangential plane. These results were compared with more complex layouts, including up to five mirrors including parabolas working in the Kirpatrick-Baez geometry.[16] The most interesting configuration analised is a beamline made by two parabolic mirrors only, placed after DW and used to generate a parallel beam both in the horizontal and the vertical planes while re-focusing is again obtained with a toroidal mirror at the end of the beamline. However, the high cost of the aspherics oriented our choice towards toroidal mirrors altough the layout of SINBAD can be easily converted to the one above described.

4. THE POLARIZATION PROPERTIES OF THE DAΦNE SOURCE AND OF THE SINBAD BEAMLINE

SR is a non-thermal source with both linear and circular polarization rate, a property of great importance in many applications. The two components σ and π of the linear polarization are characterized by the direction of the vector of the electrical radiation field: E_σ lies in the orbital plane of revolution and is directed along the radius to the centre, while the vector E_π is nearly parallel to the outer magnetic field. Actually, the total radiation power W emitted is fully polarised in the orbital plane of revolution af the electron. Since the early pioneering investigations in the visible region,[17] a lot of studies and applications have been performed at short wavelength up to the hard x-ray region, and the experiments are in good agreement with the SR theory. The component of the electrical field of the SR parallel to the orbital plane has a maximum in the orbit plane and the radiation is almost completely linearly polarized in the vicinity of this plane. Moreover SR has a circular polarisation the sign of which changes when passing through the orbital

plane. The degree of circular polarization is important for applications, because the SR emission covers with high brilliance a broad range of wavelengths. The lack of information and experimental data on the circular polarisation rate in the IR domain[18] stimulated us to calculate the polarization rate of our source using SHADOW, and ray trace our SINBAD source to the interferometer to verify the polarization rate and the flux at the end of the beamline. To evaluate the polarization we set a small slit (4 mm) at different height from the orbital plane and analized the characteristic of the source both after the slit and at the end of the beamline. To improve the quality of the simulation we introduced also the reflectivity of the goald on the description of the six mirror surfaces. Using a ray tracing with 20000 rays, we obtained for the source a very high rate of circular polarization, almost equal to one, with a transmitted flux of circularly polarized photon estimated between 5 and 10%. However, most interesting is the simulation of the spot at the end of the beamline because this layout introduces four mirror deflections in the horizontal plane and two in the vertical one with different incidence angles. The data are shown in Fig. 4, where a slit placed at about 15 mrad from the orbit should select a high degree of circular polarization (>0.8) with an estimated transmission of about 5%.

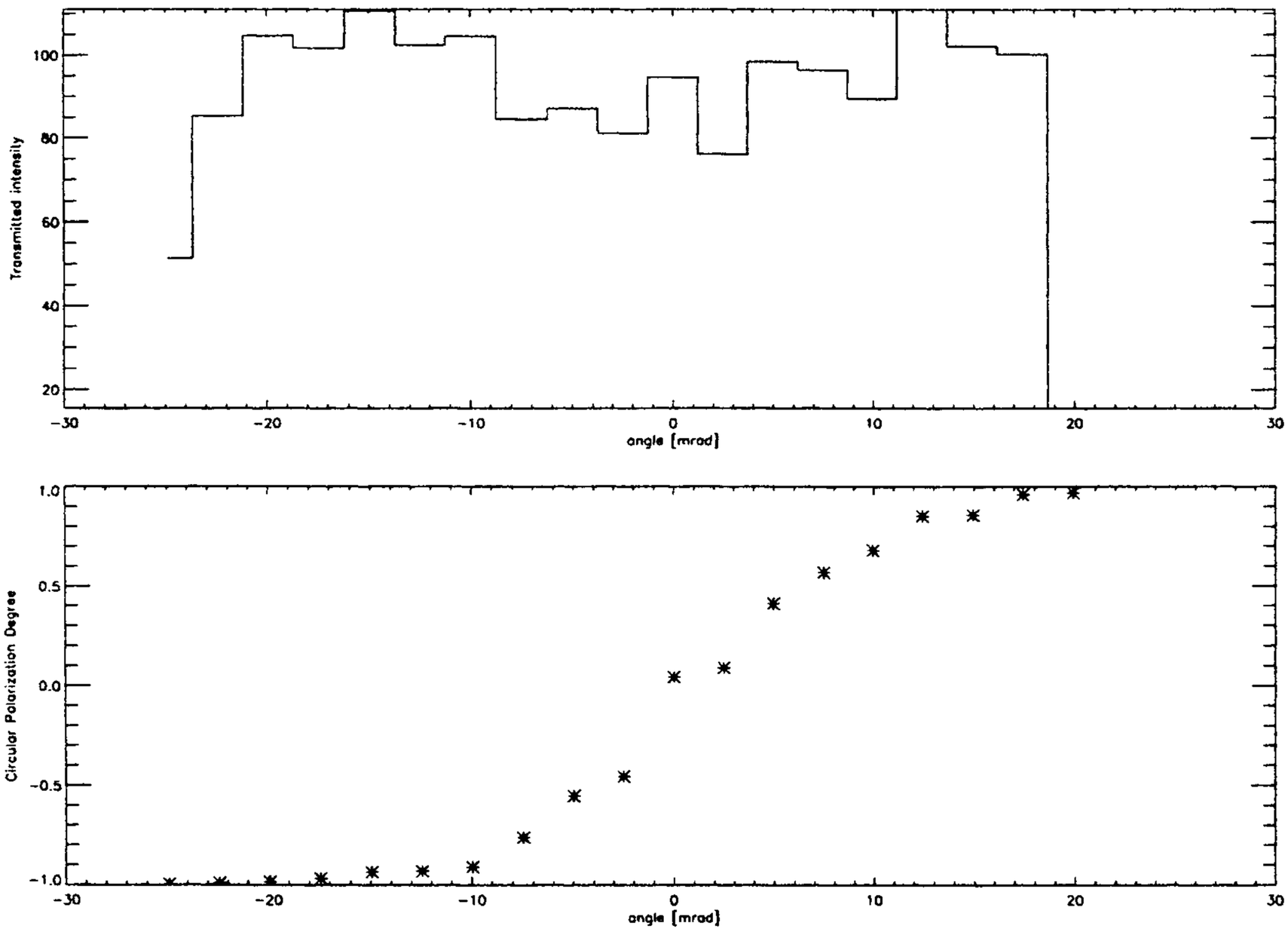

Fig 4. In the top panel the transmitted flux at 100 μm as a function of the height of the slit from the orbital plane. In the bottom panel the circular polarization rate.

5. THE ACTUAL BRILLIANCE RATIO FOR THE EXPERIMENT

At the end of the beamline a Michelson interferometer will be installed. The Actual Brilliance Ratio (ABR) of the source may give the expected gain at the sample position, i.e., inside the interferometer. In a previous paper we have already estimated the ABR between the brilliance of DAΦNE and a conventional thermal source for an ideal situation that neglected the optical system to transfer the IR radiation to the experimental area.[9] Here we estimate the ABR in the sample compartment of the interferometer. This latter is a BRUKER Equinox 55, whose optical path has been also simulated by SHADOW. The thermal source (blackbody source, subscript BB) is described as a gaussian source (σ=0.25 cm) emitting in a solid angle Ω=0.09 sterad. The calculation has been performed at λ=100 μm and the image produced by the beamline at this wavelength has been used as the source of the interferometer. Moreover, we placed several circular slits of different diameters at the focal point, in the sample compartment of the

interferometer, to test the brilliance gain defined as:

$$ABR = \frac{N^d_{SR}}{N^d_{BB}} \frac{N_{BB}}{N_{SR}} \frac{n_{SR}}{n_{BB}} \tag{6}$$

where N^d_{SR} and N^d_{BB} are the numbers of ray passing through the slit for both the synchrotron and the blackbody source respectively, N_{SR} and N_{BB} the initial number of rays and n_{SR}, n_{BB} the real number of photons emitted by the two sources. The real number of photons n_{BB} for the blackbody source may be easily estimated using the expression:

$$n_{BB} = \frac{2c10^3}{\lambda^3 \left(e^{\frac{\beta hc}{\lambda}} - 1\right)} S\Omega \qquad photons \quad 0.1\%bw/sec \tag{7}$$

being S and Ω the surface and the solid angle of emission respectively. We assumed for the surface area the value S=0.45 cm^2. The number n_{SR} of the photons emitted by our bending magnet can be obtained from the expression of the emission curve of the SR, written in terms of the Bessel function G_1:

$$n_{SR} = 1.256 \quad 10^7 \gamma G_1 \left(\frac{\lambda_c}{\lambda}\right) \qquad photons \quad 0.1\%bw/(mrad \quad mA \quad sec) \tag{8}$$

Because higher apertures may cause spurios reflections and loose of resolution, in all experiments, in particular those where small samples are investigated, the pupil size of a commercial interferometer may be varied from 0.5 mm to 5 mm of diameter. The results for the ABR with different pupils are reported in Table 6 at λ=100μm but do not agree with previous calculations,[6,9] and deserve some comments.

Table 6. ABR at λ=100 μm for different slit size.

Slit diameter (cm)	ABR
0.3	5.6
0.2	9.5
0.1	17.4
0.05	24.3

The estimate of the actual numbers of photons emitted by a blackbody is affected by a significant incertitude. The values reported in Table 6 are obtained by considering the upper limit for the BB emission. In addition, we did not consider in our simulation all the multiple reflections along the optical path of the beamline. As a consequence, at this wavelength our estimations are really lower limits for the ABR. It is noteworthy to notice that similar calculations performed at longer wavelengths, i.e., λ=1000 μm, give ABR values >200.

ACKNOWLEDGEMENTS

The authors wish to thank H. Buys, D. Cannavo', G. Cappuccio, A. Grilli, A. Raco, S. Simeoni, R.S. Sussmann and G.P. Williams for useful discussions and technical suggestions. This work has been partially supported by the UE HC&M contract 94-0551 project.

REFERENCES

1. Bassetti M., Biagini M.E., Biscari C., Guiducci S., Masullo M.R. and Vignola G., *DAΦNE*, Technical Note L-1 (1991)
2. Biagini M.E., Guiducci S., Masullo M.R. and Vignola G., *DAΦNE*, Technical Note L-4 (1991)
3. DAΦNE Machine Project, *LNF-92/033 (P)* 1992
4. Lee-Franzini J., *LNF-94/077 (P)* 1994
5. Hulbert S.L. and Weber J.M., *Nucl. Instr. Meth.* **A319** p. 25, 1992

6. Nucara A., Calvani P., Marcelli A. and Sanchez del Rio M., *LNF Report 94/053 (IR)* 1994
7. X Ray Data Booklet, Center for x-ray optics, Lawrence Berkeley Laboratory, University of California (1986)
8. Welnak C., Chen G.J., Cerrina F., *Nucl. Instr. Meth.* **A347** p. 344, 1994
9. Nucara A., Calvani P., Marcelli A. and Sanchez del Rio M., *Rev. Sci. Instr.* **66** p. 1934, 1995.
10. Burattini E., Cappuccio G. , Marcelli A., Calvani C., Nucara A. and Sanchez del Rio M., *Nucl. Instr. Meth.* **A347** p. 308, 1994.
11. Sanchez del Rio M. and Marcelli A., *Nucl Instr. and Meth.* **A319** p. 170, 1992.
12. Smither R. K., *Nucl. Instr. Meth.* **A291** p. 286, 1990.
13. Slater D.A., Hollins P., Chesters M.A., Pritchard J., Martin D.H., Surman M., Shaw D.A., and Munro I.H., *Rev. Sci. Instr.* **63** p. 1547, 1992.
14. Roy P., Mathis Y.-L., Gerschel A., Marx J.-P., Michaut J., Lagarde B. and Calvani P., *Nucl. Instr. Meth.* **A325** p. 568, 1993.
15. Nelander B., *Vibrational Spectroscopy* **9** p. 29, 1995.
16. Ambrogini R., *Thesis* University *La Sapienza*, Roma, 1997.
17. Ado Yu M. and Cherenkov P. A., *Sov. Phys. Dokl.* **1**, p. 517, 1957.
18. Stevenson James R., Ellis H. and Bartlett R., *Appl. Opt.* **12**, p. 2884, 1973.